Journal of Archaeological Science: Reports 33 (2020) 102457

Contents lists available at ScienceDirect

Journal of Archaeological Science: Reports

journal homepage: www.elsevier.com/locate/jasrep

Pyrotechnological knowledge in the pre-Hispanic Maya society: Magnetic and infrared spectrometry surveys of limekilns in the western Yucatan Peninsula (Mexico)

Avto Goguitchaichvili[a,*], Soledad Ortiz-Ruiz[b], Juan Morales[a], Vadim A. Kravchinsky[c], Oscar de Lucio[b], Rubén Cejudo[a], Rafael Garcia[a], Eunice Uc González[d], José Luis Ruvalcaba[b], Luis Barba Pingarrón[e]

[a] Servicio Arqueomagnético Nacional, Instituto de Geofísica, UNAM, Unidad Michoacán, Campus Morelia, Antigua Carretera a Pátzcuaro No. 8701 Col. Ex-Hacienda de San José de la Huerta, 58190 Morelia, Michoacán, México

[b] Laboratorio Nacional de Ciencias para la Investigación y la Conservación del Patrimonio Cultural-Instituto de Física, Universidad Nacional Autónoma de México, apartado postal 20-36401000, Ciudad de México, México

[c] Geophysics, Department of Physics, University of Alberta, Edmonton, Alberta T6G2E1, Canada

[d] Centro INAH-Yucatán, Instituto Nacional de Antropología e Historia, Km 6.5 Carretera Mérida-Progreso, Prolongación Montejo, Colonia Gonzalo Guerrero, C.P. 97310 Mérida, Yucatán, México

[e] Laboratorio de Prospección Arqueológica, Instituto de Investigaciones Antropológicas, Universidad Nacional Autónoma de México, Circuito Exterior, Ciudad Universitaria, Coyoacán, C. P. 04510 Ciudad de México, México

ARTICLE INFO

Keywords:
Infrared spectrometry
Limekilns
Paleotemperatures
Archaeomagnetism
Yucatan

ABSTRACT

Lime production structures and their combustion were investigated in the western Yucatan Peninsula (Mexico). Limekilns were excavated and the specific calcination temperature for each kiln was calculated using Fourier transform infrared spectroscopy (FTIR). A temperature range of 750–850 °C was estimated for the furnaces used for lime production. This unambiguously confirms the thermoremanent origin of magnetization carried by kiln samples and thus the validity of archaeomagnetic dating. Rock-magnetic and magnetic studies were carried out on eight well-identified limekilns. Archaeomagnetic dating based on the full geomagnetic field vector indicated that five of the kilns were last used between 900 and 1050 CE and three of the kilns were used between 1460 and 1630 CE. The absolute chronology provided in the present study is linked to the constructive splendor in the northern plains of the Maya area.

1. Introduction

The remains of ancient limekilns used by pre-Hispanic Maya communities were dated using magnetic methods. The lime production process requires temperatures generally above 750 °C which makes limekilns an excellent material to record both geomagnetic field directions and intensity during the last cooling. Lime production in Mesoamerica has been studied mainly in Teotihuacán and Maya area, with some studies in Puebla and Tlaxcala (Ortiz-Ruiz, 2019, review). However, the studies directly dealing with pyrotechnology are almost inexistent. Evidence of combustion to produce lime has been noted by archaeologists since the 1970s (Seligson et al., 2019), but systematic studies of limekilns in Mesoamerica began only five years ago (Ortiz-Ruiz et al., 2015; Rodas-Cruz, 2018; Seligson, 2016). A detailed investigation of ancient lime production − including characterization of the components of the lime mixtures and dating of the flattened floors and mortar in the kilns − was presented in Hueda-Tanabe et al. (2004). Murakami (2016) concluded that social changes in Mesoamerica were reflected in the consumption and production of lime in Teotihuacán. However, no limekilns have been reported in Teotihuacan (Barba-Pingarrón and Córdova-Frunz, 2010).

Archaeometric studies suggest that the numerous limekilns in the Maya area on the Yucatan peninsula were dedicated to the production of lime (Seligson et al., 2019; Barba-Pingarrón, 2013; Ortiz-Ruiz, 2019, 2014). Martin-Arana (1987) and Grove and Cyphers-Guillén (1987) reported three underground kilns corresponding to the classic period in Chalcatzingo. In Tepeaca, Castanzo and Anderson (2000) documented 37 lime production furnaces associated with housing platforms, two of which were dated at 1000 ± 90 yr B.C. In the Maya region in Mexico, a furnace in Copan that was probably used to produce lime was

* Corresponding author.
E-mail address: avto@geofisica.unam.mx (A. Goguitchaichvili).

https://doi.org/10.1016/j.jasrep.2020.102457
Received 4 March 2020; Received in revised form 19 June 2020; Accepted 22 June 2020

reported in Abrams and Freter (1996). Freidel and Sabloff (1984) reported the presence of a kiln in Cozumel, located in the municipality of Aguada. As the kiln was in front of an altar, the authors postulated that it was used to produce lime. Limekilns were reported in the Pulltrouser Swamp in Belize (Villaseñor-Alonso and Barba-Pingarrón, 2012) and in Cauinal (Fauvet-Berthelot, 1986). Sabloff and Tourtellot (1991) reported circular structures that the authors considered to be limekilns. All these studies propose the presence of kilns in well-defined archaeological contexts. However, no pyrotechnological or systematics archaeomagnetic investigations have been available until now. Ortiz-Ruiz et al. (2015) combined pyrotechnological and archaeomagnetic techniques to study limekilns excavated in the Maya area of Mexico. Evidence from Kiuic, in the northern Ichkaantijoo region, suggests that the kilns were pyrotechnological structures dedicated to the production of lime. Typological and production differences described in Seligson et al. (2019) suggest that lime production in the Maya area in Mexico consisted of multiple regional sub-industries interacting with each other.

We sampled eight well-identified limekilns west of the Yucatan Peninsula to estimate the paleotemperatures associated with lime production and to determine the chronology of lime production.

2. Limekiln sites and sample collection

The limekilns discovered in the ancient Maya lowlands are typically circular structures built directly on the ground; only in the case of Mérida was a kiln built inside the platform room. The construction of a kiln begins by excavating a hole at an average depth of 1.5 m; the hole is then covered with a limestone wall. At the top of the wall an annular bench is built that surrounds the hollow.

Fig. 1 shows geographic distribution of some of the kilns excavated during the archaeological rescue campaign at the western part of the Yucatan Peninsula. The kilns were deep pits in the ground, occasionally filled with layers of sediments and gravel (Fig. 2). The floor and walls of the kilns were comprised of sedimentary limestone. We sampled eight limekilns that had preserved circular architectonical features. The structural and technological similarity of the kilns suggests that they were built during the same time period. Pyrotechnological evidence inside the furnaces contained lime concretions and sediments with micro-remains of coal, ash, and fragments of calcined rock. The kiln walls presented fractures caused by their multiple exposures to high temperature.

Four of the studied limekiln sites are distributed along Federal Highway 180 (Fig. 1); four other sites are located near La Sombrilla, Vicente Guerrero, Santa Barbara (close to Maxcanu village), and Dzoyilá at Merida, the capital city of Yucatan State. Twelve or more standard paleomagnetic cores (112 samples in total) were drilled using the portable Pomeroy (*ASC Scientific*) drill and oriented using both magnetic and sun compasses. To remove, at least partly, the potential viscous remanent magnetization, all samples were stored in a magnetic shield with a residual field less than 15 nT for three weeks before taking laboratory measurements.

3. Laboratory methods and analysis

The specific calcination temperature range for each limekiln sample was determined using attenuated total reflection Fourier transform infrared spectroscopy (ATR-FTIR). ATR-FTIR enables material identification by measuring the vibration of molecular bonds (Gueta et al., 2007). Here, we obtained mineral characterization and identified physical changes in materials exposed high temperatures during lime

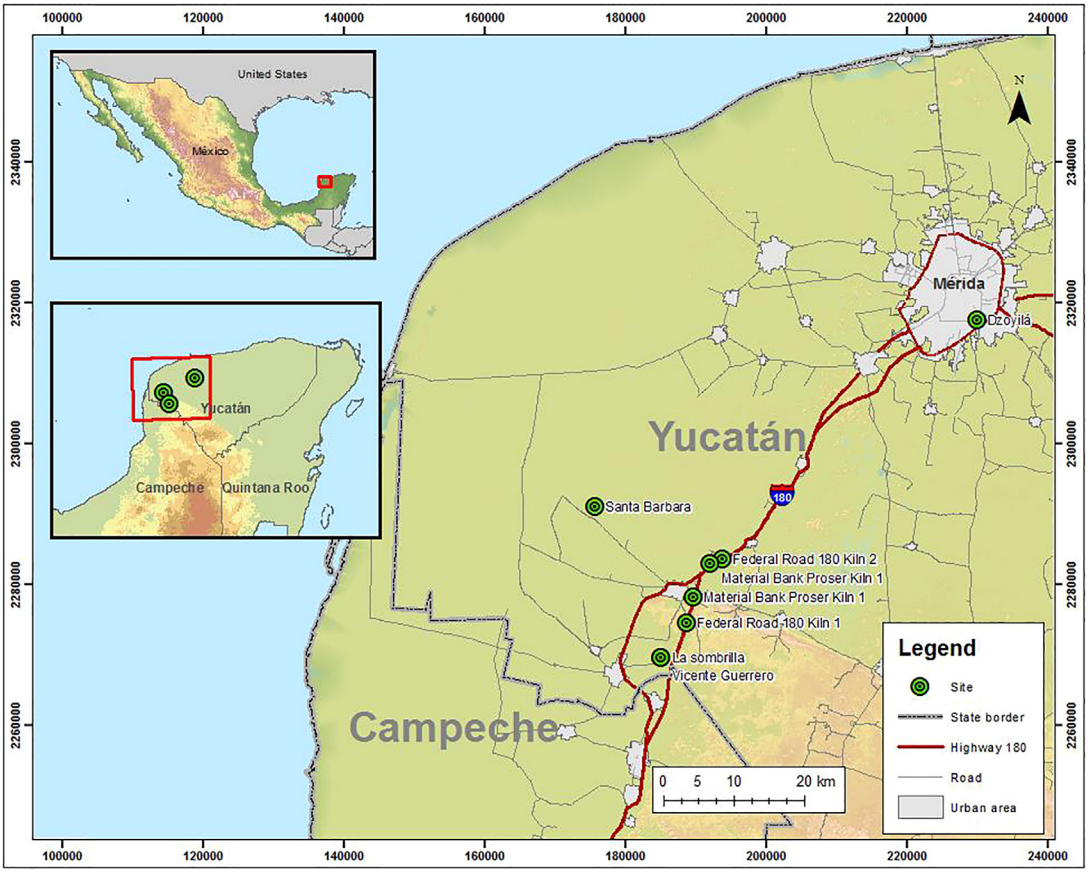

Fig. 1. Schematic map of the western Yucatan peninsula showing the location of the studied limekilns. Most of the limekiln sites are distributed along Federal Highway 180, with other sites are located near La Sombrilla, Vicente Guerrero, Santa Barbara (close to Maxcanu), and Dzoyilá at Merida, the capital city of Yucatan State.

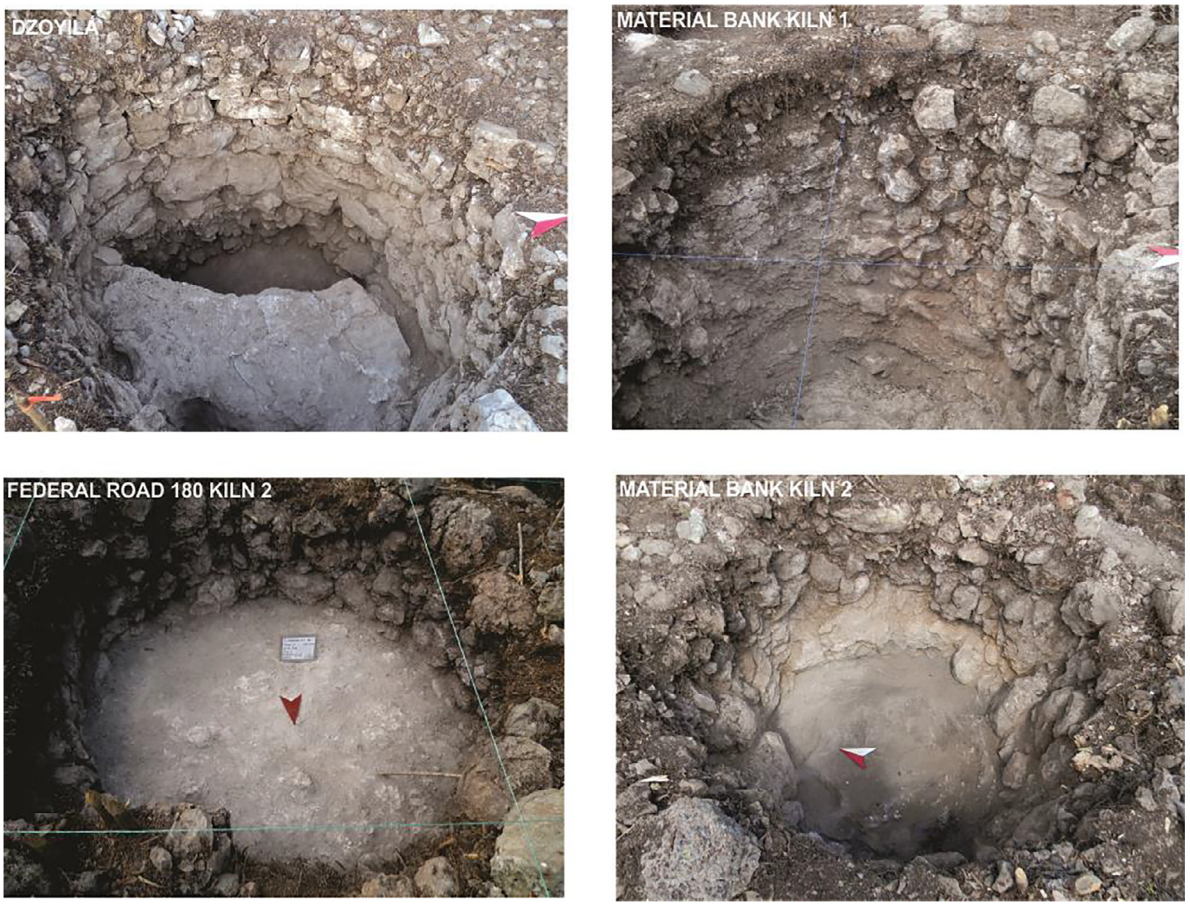

Fig. 2. Views of representative limekilns. Each kiln comprised a well-marked cavity in sedimentary rock. The construction apparently took advantage of a cavity in the mother rock and used to form the walls and floor of the kiln.

production. This technique has been applied in archaeology to study materials exposed to fire (Berna et al., 2007; Chu et al., 2008; Regev et al., 2010; Toffolo and Boaretto, 2014; Toffolo et al., 2017; Weiner, 2010).

Each sample was ground using a mortar and agate pistil to produce a fragment of 0.5–1 cm in diameter, which was place in an Eppendorf tube. The sample fragments were analyzed with a Bruker Alpha Platinum portable spectrometer in ATR mode with a diamond crystal. Spectra were obtained at a resolution of 4 cm^{-1} using 32 scans with wavenumbers in the range of 400 − 4000 cm^{-1} at the National Science Laboratory for the Research and Conservation of Cultural Heritage (LANCIC-Institute of Physics, UNAM).

Mineralogical identification was achieved by comparing the sample spectra with certified reference materials from the National Institute of Standards and Technology, SRM 88b and SRM 1D (Chukanov, 2014; Aldeias et al., 2019; Weiner, 2010). Calcination temperatures in the limekilns were determined using the methodology proposed by Chu et al. (2008) and Regev et al. (2010). This allowed us to determine the molecular changes when the materials were directly exposed to fire. Samples were analyzed by ATR-FTIR to establish the parameters of ratio ν^2/ν^4 with local materials. A calibration curve was created using the calcination temperatures of geological materials (Ortiz-Ruiz, 2019; Ortiz-Ruiz et al., in preparation).

During archaeological excavations, at least 10 samples were collected from each kiln following a stratigraphic sequence. The samples consisted of fragments of stones, sediments, and calcined rock pieces inside the kilns. Paleomagnetic cores were drilled at almost same areas in each kiln, thus, there is direct relationship between the paleomagnetic and FTIR fragments analyzed.

Saturation induced magnetization versus temperature (continuous thermomagnetic curves), hysteresis cycles, and isothermal remanent magnetization curves were recorded using a variable field translation balance (VFTB), also known as Curie balance. Natural remanent magnetizations were measured using a JR6-A AGICO spinner magnetometer, and alternating field treatments were performed with a LDA-3 demagnetizer with a maximum field of 95 mT. Primary characteristic remanent magnetization (ChRM) directions were computed using a principal component analyses (Kirschvink, 1980) of linear segments that pointed to the origin of the Zijderveld diagram and represented at least five alternating field demagnetization steps. The site-mean archaeomagnetic direction of each limekiln was obtained using Fisher statistics (Fisher, 1953). As alternating field treatments efficiently removed secondary magnetizations, these treatments were used to separate primary remanent magnetization components.

Archaeointensity experiments were performed on the samples using Coe's (1978) modification of the double heating Thellier method (Thellier and Thellier, 1959). A TD48 ASC thermal demagnetizer equipped with coils was used for these experiments. Measurements were made in 11 or 12 temperature steps between room temperature and 515–540 °C. Only three controlled heatings, i.e., partial thermoremanent magnetization (pTRM) checks at key temperatures were performed to minimize thermal remanent magnetization alterations in the samples during multiple heatings. The samples were cooled down naturally, thus no cooling rate correction was applied. The Thellier double heating technique is inconvenient because of the many heating steps (usually more than 20) required. Additionally, three to five controlled heatings (pTRM checks) and three additional heatings for the cooling rate experiments are required, which may alter the original remanent magnetization. Conventional anisotropy correction requires at least six additional heatings at high temperatures, and usually less

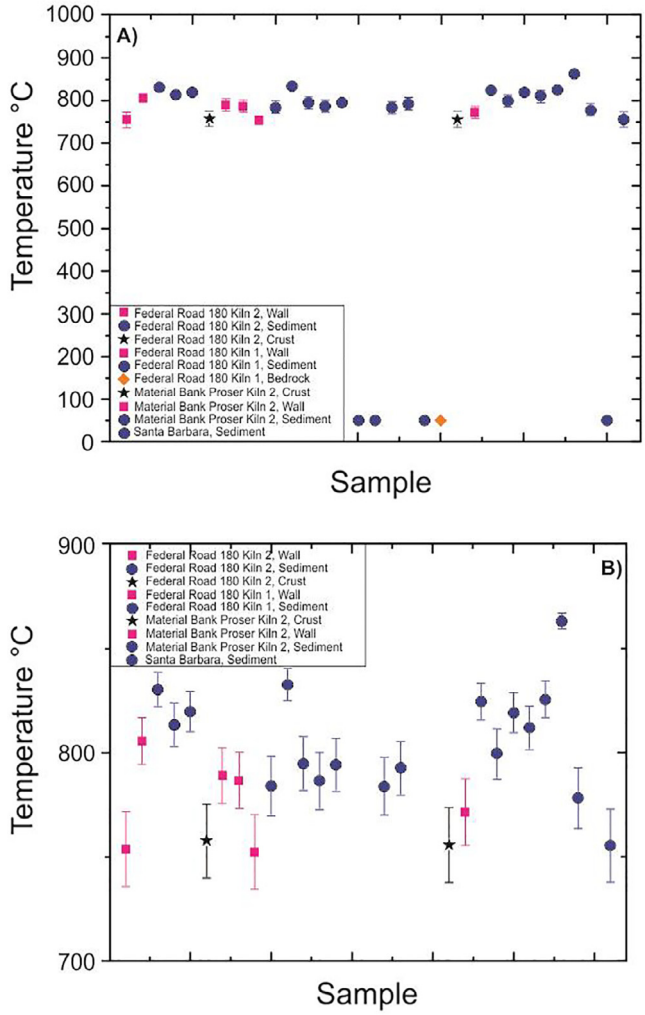

Fig. 3. Calcination temperatures estimated by Fourier transform infrared spectroscopy (FTIR). The experiments were carried out with the total attenuated reflectance (ATR) module. (b) is the enlarged (a).

than 10–15% of the original magnetization survives this treatment. To avoid such potential alterations, we measured anhysteretic remanent magnetization (ARM) instead of TRM at six positions under the simultaneous action of 90 mT alternating and 50 mT direct magnetic fields. The maximum remanence anisotropy correction factor was within 1.6% (mostly within 1.2%), therefore, we considered our samples to be magnetically isotropic, and no anisotropy correction was applied to the intensity values.

4. Results

The calcination temperatures of the samples from the studied limekilns were obtained with ATR-FTIR using the specific calibration curve for limestone materials. Samples from the interior of the limekilns had been exposed to temperatures between 750 °C and 850 °C (Fig. 3). Such temperatures are typical in lime fabrication in pyrotechnological kilns. Seligson et al. (2017) replicated a kiln in Kiuic and experimentally burned limestone with the help of Mayan artisans who are familiar with the production of lime by traditional methods. Temperatures between 800 °C and 830 °C were reached during the limestone burning. FTIR analysis of these samples yielded an average temperature of 786 °C (Ortiz-Ruiz, 2019). Previous work describing lime production by Schreiner (2002), Russell and Dahlin (2007), and Villaseñor-Alonso and Barba-Pingarrón (2012), suggest that calcination temperatures were 800–900 °C. Such calcination temperatures confirm the thermoremanent origin of remanent magnetization in the studied samples. The main magnetic carriers responsible for remanence are ferromagnetic Ti-poor titanomagnetites (almost magnetite). The thermoremanent origin of primary magnetization, obtained during the last use (heating then cooling) of a kiln, is ensured by a heating temperature above 750 °C, that is, above the Curie temperatures of magnetite and hematite. A few samples appeared to have no thermal footprint; ATR-FTIR examination showed their temperatures to have been below 50 °C (Fig. 3a). Samples with no thermal footprint were likely in positions remote from fire exposure. These samples may not carry any thermoremanent magnetization and were thus excluded from further analysis.

Fig. 4 summarizes the rock-magnetic properties of the samples. The temperature-induced saturation magnetization curves, which are reasonably reversible, present a single ferrimagnetic phase corresponding to a Curie temperature between 545 °C and 555 °C, indicative of nearly pure magnetite or Ti-poor titanomagnetite. Both hysteresis cycles and isothermal remanent magnetization (IRM) acquisition curves were recorded up to 0.85 T. Saturation was reached applying 200 mT, which attests to the presence of relatively low coercivity ferrimagnetic grains. The typical ratios derived from the hysteresis cycles (Mrs/Ms = 0.25, Bcr/Bc = 2.15) are related to a pseudo-simple magnetic domain state (Dunlop, 2002).

Some representative, alternative field demagnetization examples are shown in the orthogonal projection diagrams of Fig. 5. Most of the samples (upper part of Fig. 5) are trending toward of origin of the diagram, defining linear uni-vectorial, normal polarity magnetization components. A minor secondary overprint of probably viscous origin was sometimes identified during the demagnetizations. Such

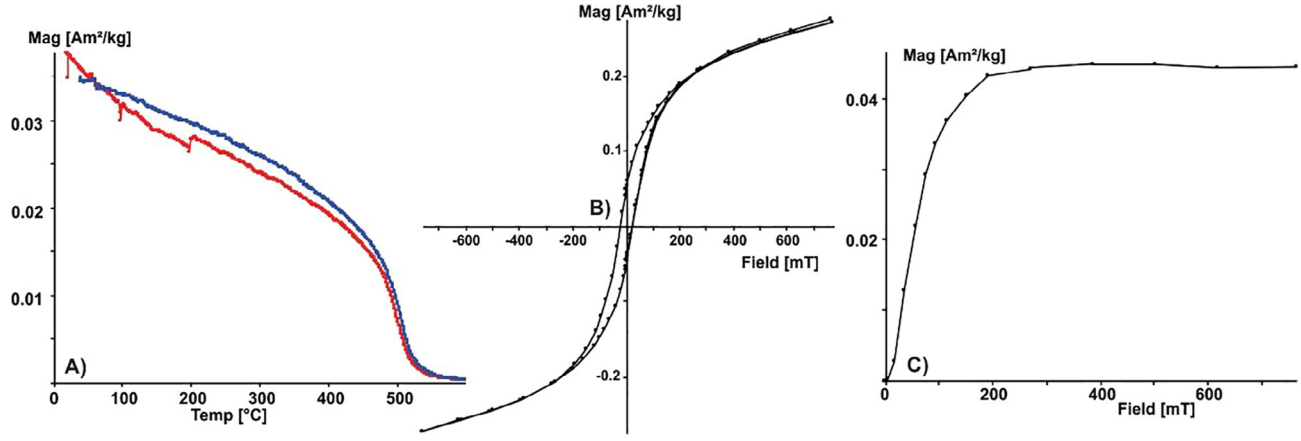

Fig. 4. A summary of rock-magnetic experiments: (a) continuous thermomagnetic curve, (b) hysteresis cycle, (c) acquisition of isothermal remanent magnetization.

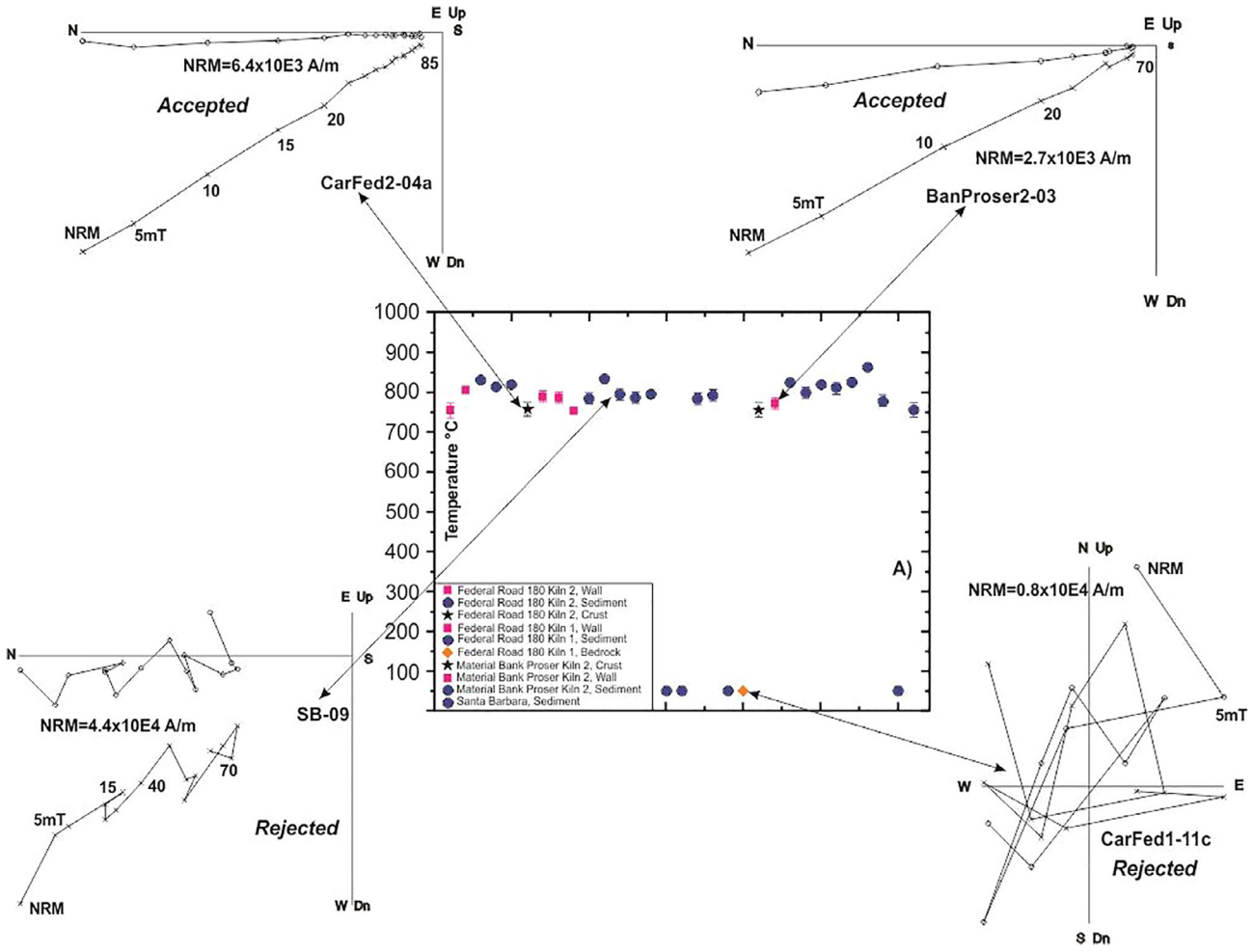

Fig. 5. Representative examples of orthogonal vector plots illustrating alternative field treatments up to 90 mT for limekiln samples. The field treatments are related to the calcination paleotemperatures obtained using ATR-FITR.

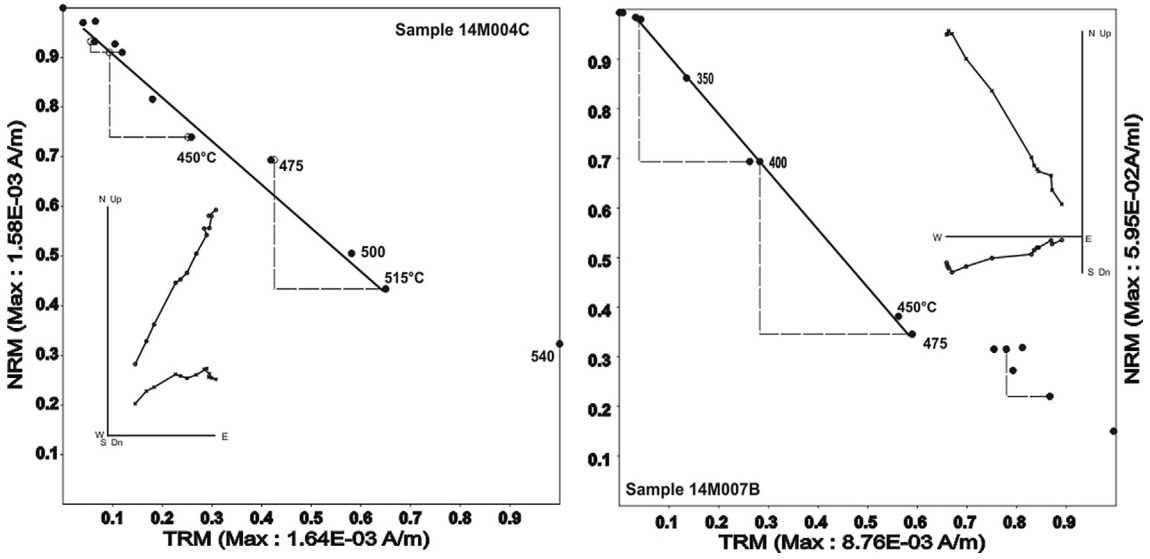

Fig. 6. Arai-Nagata plots: representative natural remanent magnetization (NRM) – thermomagnetic remanent magnetization (TRM) diagrams and associated NRM endpoint demagnetization diagrams for the representative samples.

Table 1
Directional results obtained for studied limekilns: n is the number of samples used in the calculation of the site mean direction; N is the total number of samples measured; α_{95} is the confidence cone in degrees; k is the precision parameter of the Fisher statistics; Dec. is declination; Inc. is inclination.

Site	UTM	UTM	n/N	Inc	Dec		a95 (°)	Int (tT)	Archaeomagnetic dates (A.D)
				(°)	(°)	k			
Dzoyilá	230,023	2,317,636	12/14	30.7	350.6	214	3.4	44.1 (2.6)	932–1019/1189–1281
Vicente Guerrero	185,130	2,269,632	7/10	29.9	351.8	426	3.2		934–1047/1213–1273
Santa Barbara	800,758	2,290,606	9/11	24.8	348.7	405	2.7	32.5(2.5)	912–979
Federal Road 180 Kiln 1	188,694	2,274,634	0/8						N.D.
La sombrilla	185,130	2,269,632	8/9	30.2	353.6	256	3.3		703–879/891–1004/1232-1304
Federal Road 180 Kiln 2	193,808	2,283,580	8/10	33.8	5.5	236	3.6		1498–1622
Material Bank Proser Kiln 1	189,657	2,278,236	8/11	28.1	357.4	325	4.1		707–938
Material Bank Proser Kiln 1	192,103	2,282,959	6/10	37.1	5.8	158	4.2		1459–1644

Table 2
The absolute intensity of geomagnetic field at the sample level using the Thellier-Thellier double heating method: N is the number of heating steps used; *f* is the fraction of NRM used for intensity determination; *g* is the gap factor; *q* is the quality factor as defined by Coe et al. (1978); γ is the angle between the direction of ChRM and the direction of the composite magnetization equal to NRM(*T*) if the CRM(*T*) obtained from orthogonal plots derived from Thellier paleointensity experiments is zero (Coe et al., 1984; Goguitchaichvili et al., 2015); H is the archaeointensity value and the standard deviation.

Site	LAB CODE	N	Han (μT)	± μT	γ(°)	f	g	q	Tmin-Tmax
Dzoyilá	14M001B	8	43.9	3.6	5.8	0.46	0.76	2.8	300–515
Dzoyilá	14M002C	8	44.3	3.0	3.6	0.51	0.78	6.7	300–515
Dzoyilá	14M003A	9	44.6	1.9	2.8	0.58	0.80	9.1	250–515
Dzoyilá	14M004C	10	40.8	1.6	3.2	0.52	0.82	12.5	200–515
Dzoyilá	14M005A	9	48.6	1.1	3.8	0.55	0.83	14.2	250–515
Dzoyilá	14M006A	8	42.8	1.8	4.2	0.49	0.75	6.6	300–515
St. Barbara	14M007B	6	35.2	1.2	1.8	0.64	0.84	16.8	150–475
St. Barbara	14M008C	5	29.3	2.3	3.1	0.54	0.79	8.2	200–475
St. Barbara	14M009C	6	33.9	1.7	2.6	0.66	0.82	10.2	150–475
St. Barbara	14M010C	6	32.8	1.4	3.5	0.61	0.78	11.5	150–475
St. Barbara	14M011C	5	31.5	2.8	4.3	0.53	0.81	4.3	200–475

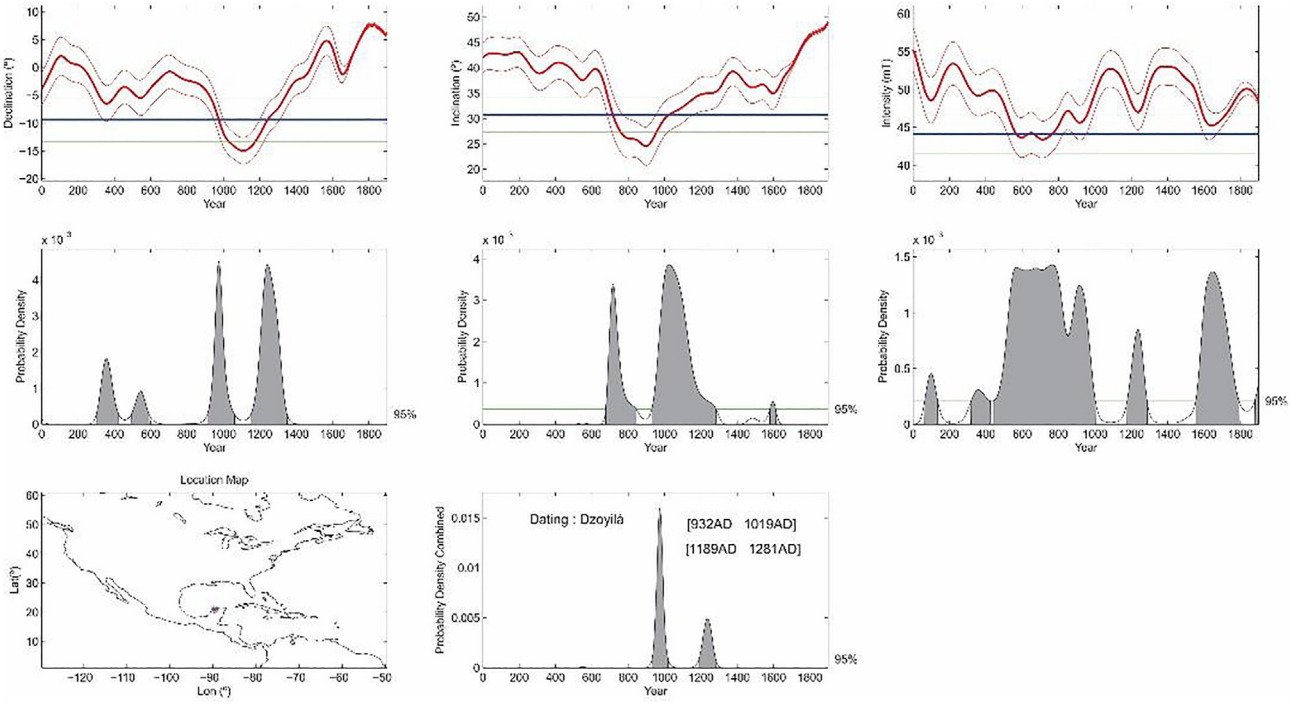

Fig. 7. Archaeomagnetic dating with a MATLAB tool provided by Pavón Carrasco et al. (2011, 2014) using a geomagnetic full vector.

components were removed by the field ≤5–10 mT. For ~80% of the analysed samples the remanent magnetization was completely removed beyond the peak alternating field of 60–80 mT. The median destructive field (MDF) ranges between 20 and 30 mT, indicating, once again, that the remanence was carried by low-coercivity minerals, most likely magnetite (Dunlop, 2002). These samples yielded a maximum angular deviation (MAD) of 0.8–4.3°. Only a few samples were rejected because of unstable behaviour during the magnetic treatments (Fig. 5, sample

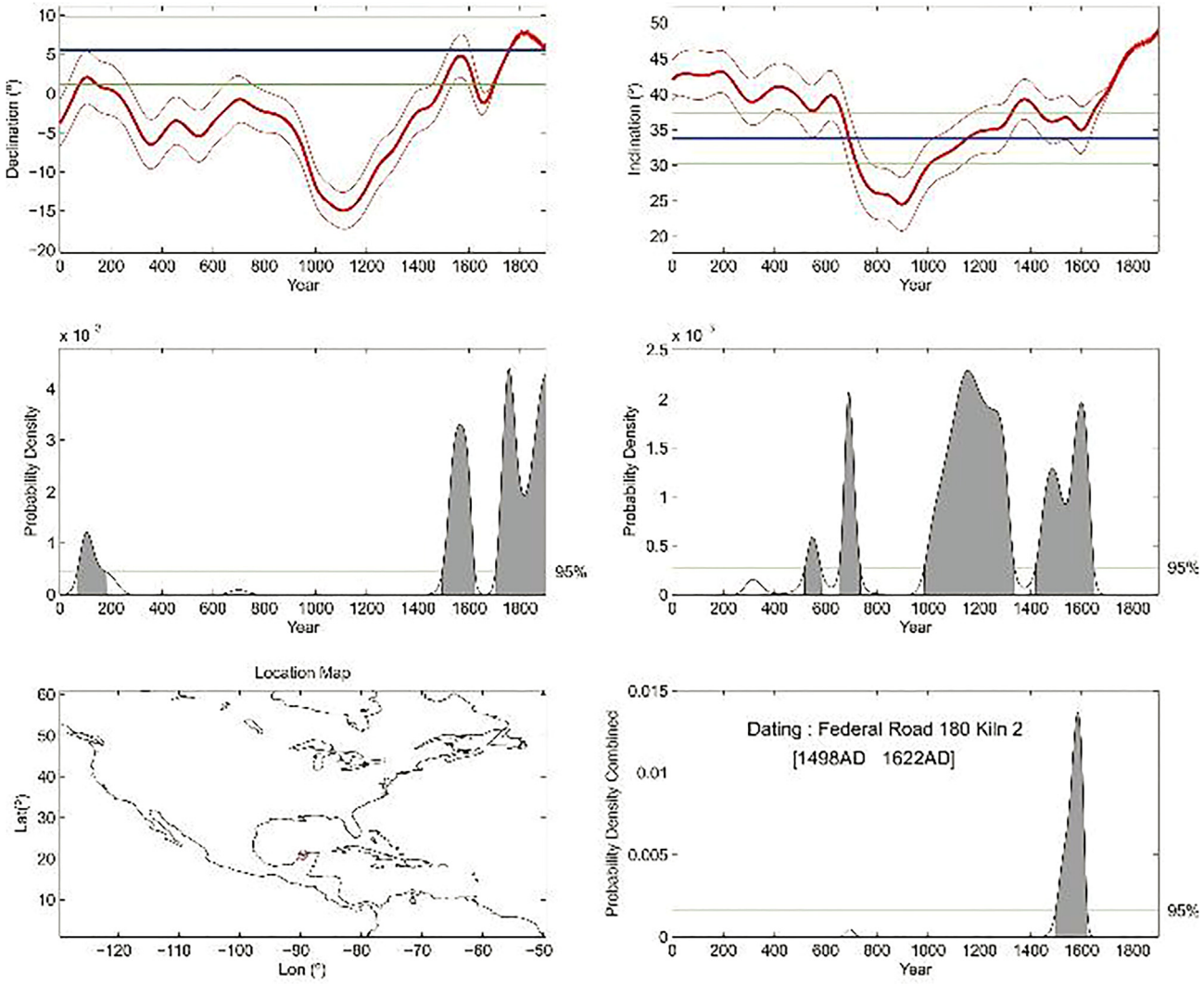

Fig. 8. Archaeomagnetic dating with a MATLAB tool provided by Pavón Carrasco et al. (2011, 2014) using only directional data.

SB09), showing MAD values above 5°. Six samples exhibited chaotic behaviour during the demagnetization without defining any linear segments (Fig. 5, sample CarFed1-11c). Such samples were from the group with no thermal footprint, as revealed by ATR-FITR analysis, and did not carry primary thermoremanent magnetization.

As absolute magnetic intensity, or archaeointensity, experiments are concerned, we accepted determinations showing no major departure of natural remanent magnetization (NRM) (the permanent magnetism of a rock or sediment) end points toward the laboratory field directions. To acquire mean values of the absolute magnetic intensity we used only samples that demonstrated low MAD. The maximum values of the angle γ between the direction of characteristic remanent magnetization (ChRM) and the direction of total magnetization, NRM(*T*), if CRM(*T*) is zero obtained from the orthogonal plots derived from the Thellier paleointensity experiments is below of 6°. We considered at least five aligned NRM removed – pTRM acquired – points (Fig. 6, Table 2). Positive partial thermoremanent magnetization (pTRM) checks were accepted within 15% for the segments from room temperature to 250–300 °C and within 10% above that temperature range. No concavity is observed on the Arai-Nagata diagrams in Fig. 6. The quality factor q, suggested by Coe et al. (1978), is generally above 5. The remanence segment *f* is about half of the total remanence for all samples.

5. Discussion and concluding remarks

Remains that have been previously heated must carry primary thermoremanent magnetization acquired during cooling from high temperatures to qualify for archeomagnetic investigation. The geomagnetic validity of the present archaeomagnetic data is supported by the fact that infrared spectroscopy yielded calcination temperatures above 750 °C in almost all cases of minerals found in limekiln samples. Site-mean paleodirections were obtained for seven limekilns (Table 1) based on 58 successful demagnetizations of 83 treated samples. The low values in the cone of confidence, α_{95}, range from 2.7 to 4.2° illustrating the high technical quality of the results. Although full demagnetization was achieved for eight standard paleomagnetic samples from limekiln 1, situated on Federal Highway 180, no directions were obtained because of the unstable and chaotic behavior of analyzed samples in alternating field treatments. Out of 24 samples analyzed in the two studied sites, only 11 samples provided acceptable absolute archaeointensity determinations. The Dzoyilá limekiln site provided an average intensity of 44.1 ± 2.6 μT, and the Santa Barbara site yielded 32.5 ± 2.5 μT.

For archaeomagnetic dating between 0 and 1900 A.D, we used the model SHADIF14k and the corresponding MATLAB tool described in Pavón Carrasco et al. (2011, 2014). A full geomagnetic vector (inclination, declination, and absolute intensity) was used in only two cases (Fig. 7) because no intensity results were obtained for the

remaining five sites; therefore, only directional data were used for age interval estimations (Fig. 8). Four sites provided a single time interval (Table 1), and two kilns yielded two different absolute ages. Three age intervals were obtained for the kiln at La Sombrilla. A time interval of 900–1050 CE was recurrent in all determinations except for sites Federal Highway 180 Kiln 2 and Material Bank Proser Kiln 2, which yielded the significantly younger ages of 1560 and 1630 CE The archaeomagnetic date indicates the last use of the heated structure, therefore, it is possible that these two kilns were rehabilitated at the beginning of the Colonial period.

The absolute chronology provided in our study allows us to refine the time of the lime manufacturing process. The interval 900–1050 CE agrees with the ceramic typology of the region (Ancona-Aragón et al., 2013), and with the data from the Kiuic ovens in the Puuc area (Seligson, 2016). In the latter study, charcoal samples from four kilns yielded an age interval of 650–900 CE (calibrated at 2 sigma). Locating the intensive use of lime production furnaces for this period is linked to the constructive splendor in the northern plains of the Maya civilization region. Seligson et al. (2019) compiled available information on limekilns in the Maya region in Mexico and placed their use in the Classic period, except for four limekilns that were dated by the radiocarbon technique. The chronology given to the other archaeological sites was essentially based on the ceramic typology. Two kilns yielded post-conquest ages, and interestingly, both were found very close to the colonial *Haciendas* which might indicate that the Spaniards produced lime to obtain construction material. These new dates allow us to identify the evolutionary steps in the modifications and adaptations of limekilns, which in some cases do not preserve any architectural pattern, only a thermal imprint.

The age ranges obtained in this study allow us to refine the chronology and duration of the lime manufacturing process. The evidence indicates intensive use of limekilns to produce lime in late Classic/Postclassic periods by the Maya people in the northern plains of the Yucatan peninsula. Previous data compiled from this area (Seligson et al., 2019) suggested that the limekilns were used principally in the Classic period. Our data indicate that some of studied kilns were used (or reused) during the colonial era. The location of the kilns near colonial towns suggests that the Spaniards used pre-Hispanic production techniques for lime production. Recent discoveries north of Yucatan suggest that modifications of the pre-Hispanic features are visible at the Maxtunil site. For instance, the open chapel built on the Maxtunil site presents pre-Hispanic materials and evidence of pre-Hispanic construction techniques (Gongora Salas, 2017). The depth and circular shape of the kilns, the modifications of bedrock to build the kilns, and the adaptations in the areas of kiln use are almost identical in historical and pre-Hispanic periods. Based on archeometric and archeological analyses, we suggest the function of the kilns was to produce lime, at least from the Late Classic period to the early years of the conquest.

Acknowledgments

This work was supported by the CONACYT project n° 252149 and DGAPA-PAPIIT grant n° IN101920. The authors acknowledge the partial support of Laboratorio Nacional de Ciencias para la Investigación y Conservación del Patrimonio Cultural (LANCIC), Institute of Physics, UNAM, and through the CONACYT Grants LN279740, LN293904, LN299076, and CB239609. V.A.K. was supported by the Natural Sciences and Engineering Research Council of Canada (NSERC Grant RGPIN-2019-04780).

References

Abrams, E., Freter, A.C., 1996. A Late Classic lime plaster kiln from the Maya Centre of Copan, Honduras, Antiquity, 70, 422–428.

Aldeias, V., Gur-Arieh, S., Maria, R., Monteiro, P., Cura, P., 2019. Shell we cook it? An experimental approach to microarchaeological record of shellfish roastingArchaeol. Anthropol. Sci. 11, 389–407.

Ancona-Aragón, I., Uc-González, E., Morales-Uh, R., 2013. Residencias Habitacionales de Elite en la Periferia de Oxkintok: La Evidencia Cerámica. Ponencia presentada en el Encuentro Internacional de los Investigadores de la Cultura Maya, Campeche, Campeche.

Barba-Pingarrón, L.A., Córdova-Frunz, J.L., 2010. Materiales y Energía en la Arquitectura de Teotihuacán. IIA, UNAM, 223 p.

Barba-Pingarrón, L., 2013. El Uso de la cal en el mudo prehispánico mesoamericano. En La Cal. Historia, Propiedades y Usos. In: Luis Barba-Pingarrón, Isabel Villaseñor-Alonso (Eds.), Universidad Nacional Autónoma de México, Instituto de Investigaciones Antropológicas, Asociación Nacional de Fabricantes de Cal A. C. México, D. F. pp. 21–47.

Berna, F., Behar, A., Shahack-Gross, S., Berg, J., Boaretto, E., Gilboa, A., Sharon, I., Shalev, S., Shilstein, S., Yahalom-Mack, N., Zorn, J.R., Weiner, S., 2007. Sediment exposed to high temperatures: reconstructing pyrotechnological processes in late bronze and iron age strata at Tel Dor (Israel). J. Archaeol. Sci. 34, 358–373.

Castanzo, R.A., Anderson, J.H., 2000. Formative period lime kilns in Puebla, México, Mexicon, XXVI, pp. 86–90.

Chu, V., Regev, L., Weiner, S., Boaretto, 2008. Differentiating between anthropogenic calcite in plaster, ash and natural calcite using infrared spectroscopy: implications in archaeology. J. Archaeol. Sci. 35, 905–911.

Chukanov, N.V., 2014. Infrared Spectra of Mineral Species. Extended library. Springer, p. 1726.

Coe, R.S., Grommé, S., Mankinen, E.A., 1978. Geomagnetic paleointensities from radiocarbon-dated lava flows on Hawaii and the question of the Pacific nondipole low. J. Geophys. Res.: Solid Earth 83 (B4), 1740–1756.

Coe, R.S., Gromme, S., Mankinen, E.A., 1984. Geomagnetic paleointensities from excursion sequences in lavas on Oahu, Hawaii. J. Geophys. Res.: Solid Earth.

Dunlop, D.J., 2002. Theory and applications of the Day plot (Mra/Mr versus Hcr/Hc). Theoretical curves and test using titanomagnetite data. J. Geophys. Res. 107, 1029–2001.

Fauvet-Berthelot, M.F., 1986. Ethnopréhistoire de la maison maya: Guatemala 1250-1525, CEMCA, p. 281.

Freidel, D., Sabloff, J., 1984. Cozumel. Late Maya Settlement Patterns. Academic Press, p. 208.

Fisher, R.A., 1953. Dispersión on a sphere. Proc. Royal Soc. London 217, 295–305.

Gueta, R., Natan, A., Addadi, L., Weiner, S., Refson, K., Kronik, L., 2007. Local atomic order and infrarred spectra of biogenic calcite. Angew. Chem. Int. Ed. 46, 291–294.

Goguitchaichvili, A., Morales, J., Schavelzon, D., Vásquez, C., Gogorza, C., Loponte, D., Rapalini, A., 2015. Variation of the Earth's magnetic field strength in South America during the last two millennia: new results from historical buildings of Buenos Aires and Re-evaluation of regional data. Phys. Earth Planet. Interiors 245, 15–25.

Gongora Salas, A., 2017. Maxtunil: Pueblo legendario de Nakuk Pech. In: Aportaciones del Salvamento arqueologico y otros estudios en la Reconstruccion de la Cultura Maya. Memorias del Tercer Simposio de Cultura Maya Ichkaantijoo, editado por A. Góngora Salas, pp. 111–128.

Grove, D.C., Cyphers-Guillén, A., 1987. The Excavations. In: Grove, D.C. (Ed), Ancient Chalcatzingo, University of Texas Press, pp. 21–55.

Hueda-Tanabe, Y., Soler-Arrechalde, A.M., Urrutia-Fucugauchi, J., Barba, L., Manzanilla, L., Rebolledo-Vieyra, M., Goguitchaivhvili, A., 2004. Archaeomagnetic studies in central mexico-dating of mesoamerican lime-plasters. Phys. Earth Planet. Interiors 147, 269–283.

Kirschvink, J.L., 1980. The least-squares line and plane and the analysis of palaeomagnetic data. Geophys. J. Royal Astron. Soc. doi.org/10.1111/j.1365-246X.1980.tb02601.x.

Martin-Arana, R., 1987. Classic and Posclassic Chalcatzingo. In: Grove, D.C. (Ed.), Ancient Chalcatzingo, University of Texas Press, pp. 387–399.

Murakami, T., 2016. Materiality, regimes of value, and the politics of craft production, exchange, and consumption: a case of lime plaster at Teotihuacan, Mexico. J. Anthropol. Archaeol. 42, 56–78.

Ortiz-Ruiz, M.S., 2019. El conocimiento pirotecnológico de la sociedad Maya Prehispánica: estudio de los hornos para cal en las Tierras Bajas Mayas del Norte, Tesis de doctorado, UNAM.

Ortiz-Ruiz, M.S., 2014. Caracterización de las estructuras anulares de la región Occidente de las Tierras Bajas Mayas. Tesis de Maestría. El Colegio de Michoacán A. C.

Ortiz-Ruiz, S., de Lucio, O.G., Mitrani-Viggiano, A., Pérez-Castellanos, N.A., Ruvalcaba-Sil, J.L., Barba-Pingarrón, L., in prep. Maya Fire: Calibration Curve for the measurement of Calcination Temperatures of Limestone, Lime and Related Materials by FTIR measurements.

Ortiz-Ruiz, S., Goguitchaitchvili, A., Morales, J., 2015. Sobre la edad de los hornos para cal en el área Maya. Arqueología Iberoamericana 28, 9–15.

Pavón Carrasco, F., Rodríguez-González, J., Osete, M.L., Torta, J.M., 2011. A Matlab tool for archeomagnetic dating. J. Archaeol. Sci. 38, 408–419.

Pavón Carrasco, F.J., Osete, M.L., Torta, J.M., De Santis, A., 2014. A geomagnetic field model for the Holocene based on archeomagnetic and lava flow data. Earth Planet. Sci. Lett. 388, 98–109.

Regev, L., Poduska, K.M., Addadi, L., Weiner, S., Boaretto, E., 2010. Distinguishing between calcites formed by different mechanisms using infrared spectrometry: archaeological applications. J. Archaeol. Sci. 37, 3022–3029.

Rodas-Cruz, D., 2018. La cal en Tepeticpac Taxcallan: su producción y uso. Tesis de Licenciatura. Universidad de las Américas Puebla, Puebla.

Russell, B.W., Dahlin, B.H., 2007. Traditional burnt-lime production at Mayapán. J. Field Archaeol. 32, 407–423.

Sabloff, J., Tourtellot, G., 1991. The Ancient Maya City of Sayil: The Mapping of a Puuc Regional Center. Tulane University, p. 38.

Schreiner, T., 2002. Traditional Maya Lime Production: Environmental and Cultural

Implications of a Native American Technology. Dissertation, Department of Architecture, Universidad de California, Berkeley, p. 269.
Seligson, K., Ortiz-Ruiz, S., Barba-Pingarrón, L., 2019. Prehispanic Maya burnt lime production: previous studies and future directions. Ancient Mesoamerica 30, 199–219.
Seligson, K.E., 2016. The prehispanic Maya burnt lime industry: socio-economy and Environmental Resource Management in the Late and Terminal Classic Period Northern Maya Lowlands (650–950 CE). Dissertation. University of Wisconsin-Madison.
Seligson, K., Gallareta-Negrón, T., May-Ciau, R., Bey III, G.B., 2017. Lime powder production in the Maya Puuc region (A.D. 600–950): an experimental Pit-Kiln. J. Field Archaeol. 42, 129–141.
Thellier, E., Thellier, O., 1959. Sur l'intensité du champ magnétique terrestre dans le passé historique et géologique. Ann. Geophys. 15, 285–376.
Toffolo, M.B., Ullman, M., Caracuta, V., Weiner, S., Boaretto, E., 2017. A 10,400-year-old Sunken Lime Kiln from the Early Pre-Pottery Neolithic B at the Nesher-Ramla Quarry (el-Khirbe),Israel. J. Archaeol. Sci.: Rep. 14, 353–364.
Toffolo, M.B., Boaretto, E., 2014. Nucleation of aragonite upon carbonation of calcium oxide and calcium hydroxide at ambient temperatures and pressures: a new indicator of fire-related human activities. J. Archaeol. Sci. 49, 237–248.
Villaseñor-Alonso, I., Barba-Pingarrón, L., 2012. Los orígenes tecnológicos de la cal, Cuicuilco Nueva Época, 19, 11–41.
Weiner, S., 2010. Microarchaeology. Beyond the Visible Archaeological Record, Cambridge University Press, p. 414.